ARTICLE IN PRESS

Available online at www.sciencedirect.com

ScienceDirect

Advances in Space Research xxx (2020) xxx–xxx

ADVANCES IN SPACE RESEARCH
(a COSPAR publication)

www.elsevier.com/locate/asr

Characteristics of probability distribution functions of low- and high-latitude current systems during Solar Cycle 24

Bharati Kakad *, Amar Kakad

Indian Institute of Geomagnetism, New Panvel 410218, India

Received 22 August 2019; received in revised form 14 December 2019; accepted 20 December 2019

Abstract

Recent solar cycles (SCs) 21–24 have experienced a gradual decrease in their activity with considerable weakening during current SC 24. This is a unique opportunity to examine the long-term response of Earth's low-latitude ring-current and high latitude auroral electrojet current systems during such systematically decreasing solar activity. With the advancement in technology, continuous recordings of ground/space magnetic field are available for the last few decades that allow us to explore the behaviour of probability distribution functions (PDFs) linked with the ring-current and auroral electrojet current systems for past five SCs (20–24). Also, PDFs linked with solar wind parameters that drive these current systems like magnetic field and velocity at Earth's bow shock are examined. We noticed the significant narrowing of PDF of ring-current and auroral electrojet during SC 24. The number of one-hour intervals with $Dst < -150$ nT are less than 600 for SCs 20–23, which constitutes less than 0.7% of respective PDF, and number of one-hour intervals with $Dst < -250$ nT are less than 100 for SCs 20–23, which corresponds to less than 0.1% of respective PDF. But for SC 24 the $Dst < -150$ nT encountered only for 58 h, which corresponds to 0.06% of PDF and there are no intervals when Dst was < -250 nT. For auroral electrojet, the number of one-hour intervals with $AE > 750$ nT and $AE > 1500$ nT are less than 3060 and 70, respectively for SCs 20–23, which corresponds to <4% and <0.06% of respective PDFs. But for SC 24 the $AE > 750$ nT encountered only for 1398 h, which corresponds to 1.7% of PDF and there are only 9 intervals when AE increased above 1500 nT, which is 0.01% of PDF. It implies that the probability of intense ring-current and auroral electrojet current during SC 24 was unusually low. Such narrowing is seen in PDFs of the interplanetary magnetic field and solar wind velocity as well. This fair quiet space weather experienced during SC 24 is attributed to the weakening of solar activity, which has subsequently influenced the strength of the interplanetary magnetic field and solar wind velocity at Earth's bow shock.

Keywords: Ring current system; Auroral electrojet current; Distribution function; Earth's magnetosphere; Solar activity

1. Introduction

Sun is the main source of energy for our planet. From Sun we get radiations of different frequencies and energetic particles in the form of the solar wind. It is widely established that Sun's activity varies on short (few days) and long (tens of year) time scales (Echer et al., 2004; Usoskin, 2017). The most dominant periodicity which is evident in the sunspot series, the longest available observational series of Sun, is of nearly 9–11 years and known as the solar cycle (Cole, 1973; Hathaway, 2010). This cyclic activity does not have the same peak for each cycle. In fact, the peak varies with the solar cycle (SC). So far, the strongest SC had a peak sunspot number of 285 and weaker SCs had peaks of magnitude 81.2–82, which corresponds to SC 19, and SC 6–5 (falls in the Dalton minimum period), respectively (Kakad et al., 2017). These peak sunspot

* Corresponding author.
E-mail address: bkakad9@gmail.com (B. Kakad).

https://doi.org/10.1016/j.asr.2019.12.021
0273-1177/

Please cite this article as: B. Kakad and A. Kakad, Characteristics of probability distribution functions of low- and high-latitude current systems during Solar Cycle 24, Advances in Space Research, https://doi.org/10.1016/j.asr.2019.12.021

numbers are based on the newly proposed Version II sunspot series (Clette et al., 2016). Knowledge of foresight and insight of solar activity is extremely important to understand its influence on the near-Earth environment. A geomagnetic storm is one of the manifestation of space weather events, which is directly governed by the state of interplanetary plasma in the vicinity of Earth and it is mainly controlled by solar activity (Gonzalez et al., 1994; Tsurutani et al., 1997; Echer et al., 2005). Geomagnetic storms have diverse impacts on our ground and space based technologies. Its severity can be understood by taking the example of a super geomagnetic Carrington storm (Tsurutani et al., 2003). Coronal mass ejection (CME), Co-rotating interaction regions (CIRs), high speed streams (HSS), and solar flares emitted from Sun are the main sources for the modulation of interplanetary solar wind plasma during SC. However, the relative importance of each of these driving structures varies with phase of SC. There are several studies in the past relating solar wind plasma properties and the occurrence of geomagnetic storms during entire SC or different phases (ascending or descending) of SC (Gonzalez et al., 2007; Richardson, 2013; Rawat et al., 2018). In some studies, the sources (CMEs or CIRs) and geomagnetic storm characteristics have been examined to get better insights about the geoeffectiveness of these space weather events (Alves et al., 2006; Richardson et al., 2006; Borovsky and Denton, 2006; Shen et al., 2017). Gonzalez et al. (2011) have reviewed the interplanetary causes responsible for intense geomagnetic storms (*Dst* <-100nT) of SC 23 (1997–2005).

Sun has experienced a gradual decrease in its activity during SC 20–24. Sun's magnetic field has also weakened significantly over this period. Such a continuous decline in solar activity provides a unique opportunity to examine the response of different current systems operative in Earth's magnetosphere. In this context, Kakad et al. (2019) has examined the variation of different energies linked with the Sun and the Earth's magnetosphere-ionosphere systems. This study was carried out only for SCs 22–24 as per the availability of respective data sets. The ring-current is a magnetospheric current system, which is used to measure the strength of the geomagnetic storm. Generally, the *Dst* index, provided by WDC Kyoto, is used as a proxy for the ring-current. Another current system is the high latitude or auroral electrojet currents, which is measured by the *AE* index. Both *Dst* and *AE* are available since January 1957, which covers nearly five SCs (20–24). With such a long-term data series, meaningful information can be retrieved by applying scientific analysis tools. For example, recently, extreme value theory is applied to this long-term *Dst* data series and it is suggested that the highest expected value of $|Dst|$ is around 850 nT (Acero et al., 2018). However, for Carrington geomagnetic storm even higher values of *Dst* has been reported. Tsurutani et al. (2003) reported *Dst* reaching up to -1760 nT, which is consistent with the deviation of -1600 ± 10 nT in horizontal magnetic field component (i.e., ΔH) at low latitude station Colaba, India (Lakhina and Tsurutani, 2018). Thus, the limit of -850 nT suggested by Acero et al. (2018) indicates that the Carrington geomagnetic storm can be considered to have the upper limit of geoeffectiveness.

The occurrence rate of the geomagnetic storm is often examined using daily minimum *Dst* index crossing a certain threshold, for example, the number of days with $Dst_{min} < -250$ nT are examined for super intense geomagnetic storms. Here, we examine the strength of low-latitude ring-current and high-latitude auroral electrojet current systems during SCs 20–24. For this purpose, rather than picking the daily minimum value of the *Dst* or maximum value of the *AE*, we have considered all available information of *Dst* and *AE* (i.e., hourly data) to explore behaviour of the ring-current and auroral electrojet current systems over past five SCs (20–24). In particular, we have examined the variation of probability distribution function (PDF) associated with the ring-current and auroral electrojet current systems during SCs 20–24. The shape of the PDF gives information about the total time duration for which severe or moderate or weak geomagnetic activity is seen, which is determined by both occurrence rate and repeat period of geomagnetic activity. Recently, Zhuang et al. (2018) has reported that occurrence of a super geomagnetic storm is significantly reduced in the SC 24. This reduction will affect the PDF of the ring-current system, and hence it is worth exploring the response of the PDFs of ring-current and auroral electrojet current systems during the past five SCs. In addition, we have also examined the PDFs linked with the interplanetary solar wind parameters (like interplanetary magnetic field, solar wind velocity, electric field) at the Earth's bow shock. Such information will be helpful to understand the change in the state of space weather during the last five SCs. In this paper, Section 2 gives the details of the data used. The results are presented in Section 3 and discussed in Section 4. The present work is summarized and concluded in Section 5.

2. Data used

In present analysis, we have used hourly *Dst* and *AE* from WDC Kyoto (http://wdc.kugi.kyoto-u.ac.jp/). *Dst* index is the measure of strength of low latitude ring-current, which is a westward current located in the low latitudes at a radial distance of approximately 3–7R_E in the Earth's magnetosphere. Whereas, *AE* index measures the strength of high latitude electrojet current. Both these currents get enhanced during periods of geomagnetically active periods. The ring current enhances during main phase of geomagnetic storm due to convection electric field (Burton et al., 1975). Also the enhanced population of energetic particles due to particle injection from the tail side of magnetosphere contribute to ring current (Chapman, 1965). The enhancement of the convection electric field is needed to explain accumulation of the particles and the development of the ring current during the magnetic storms

Please cite this article as: B. Kakad and A. Kakad, Characteristics of probability distribution functions of low- and high-latitude current systems during Solar Cycle 24, Advances in Space Research, https://doi.org/10.1016/j.asr.2019.12.021

(Ebihara, 2019). The continuous data of *Dst* are available since January 1957- May 2019, which covers nearly six SCs (19–24). But for SC 19 the data coverage is not complete as the start time of SC 19 is April 1954. The *AE* index is available from January 1957 to February 2018. For present SC 24, WDC Kyoto has nearly 457 days less data availability of *AE* as compared to *Dst*. Apart from this we used international monthly smoothed sunspot Version-II observations from WDC-SILSO (http://www.sidc.be/silso/) to get the start time (t_s), end time (t_e) and peak smoothed sunspot number (S_m) for these SCs. Parameter S_m is considered as the measure of strength of SC. These SC characteristics are readily available in Kakad et al. (2017). It is noted that from SC 21 the peak smoothed sunspot number shows a gradual decrease for consecutive SCs (i.e., $S_m^{21} = 232.9$, $S_m^{22} = 212.5$, $S_m^{23} = 180.3$, $S_m^{24} = 116.4$). The percentage decrease in the peak smoothed sunspot number from SC 21–22, 22–23, and 23–24 are 8.6% 15.1%, and 35.6%, respectively. Such gradually declining phase of solar activity is an opportunity to explore variability of the ring-current and auroral electrojet current systems, and it is worth exploring as these current systems are directly driven by the solar wind-magnetosphere interaction and their coupling efficiency. We have used interplanetary magnetic field, solar wind velocity and dawn-to-dusk electric field at Earth's bow shock nose to understand the observed narrowing of PDFs linked with these current systems during SC 24. Hourly observations of these interplanetary solar wind parameters are taken from OMNIWEB (https://omniweb.gsfc.nasa.gov/) and it is available from January 1964 to July 2019. The variation of hourly *Dst*, *AE*, IMF *Bz*, solar wind velocity, and dawn-to-dust electric field *Ey* (+*y* is eastward) are shown in Fig. 1(a)–(e), respectively. It may be noted that there are several short (and occasionally long) duration data gaps in IMF *Bz*, and solar wind velocity for SCs 20–22. However, these gaps are not clearly visible in Fig. 1 because we have plotted the data for five SCs together. These data gaps altogether give rise to more than 33% of data loss for SCs 20–22. Also, data gaps in IMF *Bz* and solar wind velocity are not occurring at the same time, as a result total data gap in *Ey* is relatively larger. Start time of SCs 19–24 is marked by dotted vertical lines and the values of peak smoothed sunspot number for respective SCs are mentioned. In general, the *Dst* found to be > -450 nT during January 1957–May 2019 except the historic March 1989 geomagnetic storm during which *Dst* reached -589 nT. This severe geomagnetic storm caused the nine-hour outage of electricity transmission at Québec (Molinski et al., 2000). It may be noted that often instruments get saturated during severe space weather conditions and hence several data gaps can be seen in interplanetary solar wind observations as evident in Fig. 1(c)–(e). We have investigated the response of ring-current and auroral electrojet current systems together with interplanetary solar wind parameters at Earth's bow shock during these SCs. The results from the present analysis are discussed in the next section.

3. Results

Here, our aim is not to look into individual geomagnetic storm or space weather events but as a whole the response of low-latitude ring current and high-latitude auroral electrojet current systems during SCs 20–24. For this purpose we estimated the PDFs using *Dst* and *AE* data for SCs 20–24. It is noticed that the range for the *Dst* variation is -589 nT to 95 nT and for *AE* it is 0 to 3195 nT during the period of observation. For each SC we estimated separate PDF using *Dst* and *AE* observations, which are shown in Fig. 2a and b, respectively. We used the bin size of 25 nT for *Dst* and 75 nT for *AE*. As the length of each SC is slightly different, we have 100112, 92052, 84754, 110361, and 91641 one-hour values of *Dst* for SCs 20, 21, 22, 23 and 24, respectively. As there is no data loss for *Dst*, these numbers in hours actually corresponds to the length of respective SCs, which is 11.42, 10.5, 9.67, 12.59 years for SCs 20–23, respectively. It may be noted that SC 24 is still in progression, hence we do not know the exact length of the present SC. Here, 91641 h of *Dst* observations for SC 24 represent data till May 2019. The SC 24 initiated close to December 2008 and so far it has spent nearly 10.46 years. For *AE* index, there is a data loss for certain period and total duration for which *AE* observations are available, are 98271, 76349, 72324, 110361, 80673 h, and corresponding data loss is 1.7%, 17%, 14.7%, 0%, 0%, for SCs 20–24 respectively. In spite of the data loss we can rely on the PDFs estimated from *AE* as the data loss is not too high (<18%).

Presently, the SC 24 is almost in its ending phase and it is suggested that it may cease close to 2020 (Kakad et al., 2017). The panel of solar experts has also suggested that the current SC 24 come to an end close to late in 2019 or 2020 (see https://www.weather.gov/news/190504-sun-activity-in-solar-cycle). Thus, we can say that the observations of *Dst* and *AE* encompass maximum period of SC 24 and hence the derived PDF can be assumed to represent the scenario similar to that of complete SC 24. In Fig. 2a and b it is clearly seen that the PDF of *Dst* and *AE* for the SC 24 have experienced significant narrowing as compared to the PDFs associated with SCs 20–23. Overall there are no time intervals with $Dst < -225$ nT and there are hardly 9 h when *AE* is slightly above 1500 nT during the SC 24.

As the number of *Dst* observations are different in different SCs we can not compare these PDFs. Thus, we obtained the normalized probability distribution function (NPDF). The NPDF is obtained by dividing the PDF by total number of available one-hour observations in that SC. Thus, the sum of NPDF will be always 1 that represents 100%. For SCs 20–24, the variation of NPDF (in %) is shown in Fig. 3(a)–(e) for *Dst* and Fig. 3(f)–(j) for *AE*, respectively. As the NPDF is depicted in % the sum of NPDF adds to 100%, which corresponds to all available observations for that SC. The comparison of NPDFs shown in Fig. 3 manifests considerable narrowing of PDFs

Please cite this article as: B. Kakad and A. Kakad, Characteristics of probability distribution functions of low- and high-latitude current systems during Solar Cycle 24, Advances in Space Research, https://doi.org/10.1016/j.asr.2019.12.021

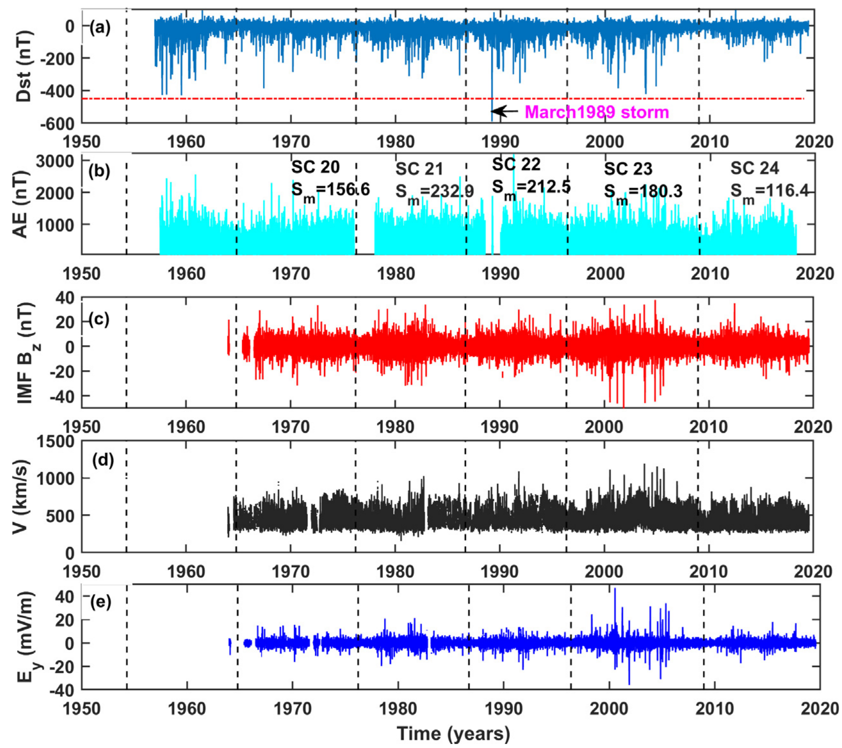

Fig. 1. Hourly values of *Dst* (a measure of the strength of low latitude ring-current system), *AE* (a measure of auroral electrojet current), IMF *Bz*, solar wind velocity, and dawn-to-dusk interplanetary electric field are plotted as a function of time. *Dst* is available from January 1957 to May 2019, *AE* is available from January 1957 to February 2018. Interplanetary solar wind parameters are at the Earth's bow shock nose and they are available from January 1964 to July 2019. It nearly covers the period of five SCs 20–24.

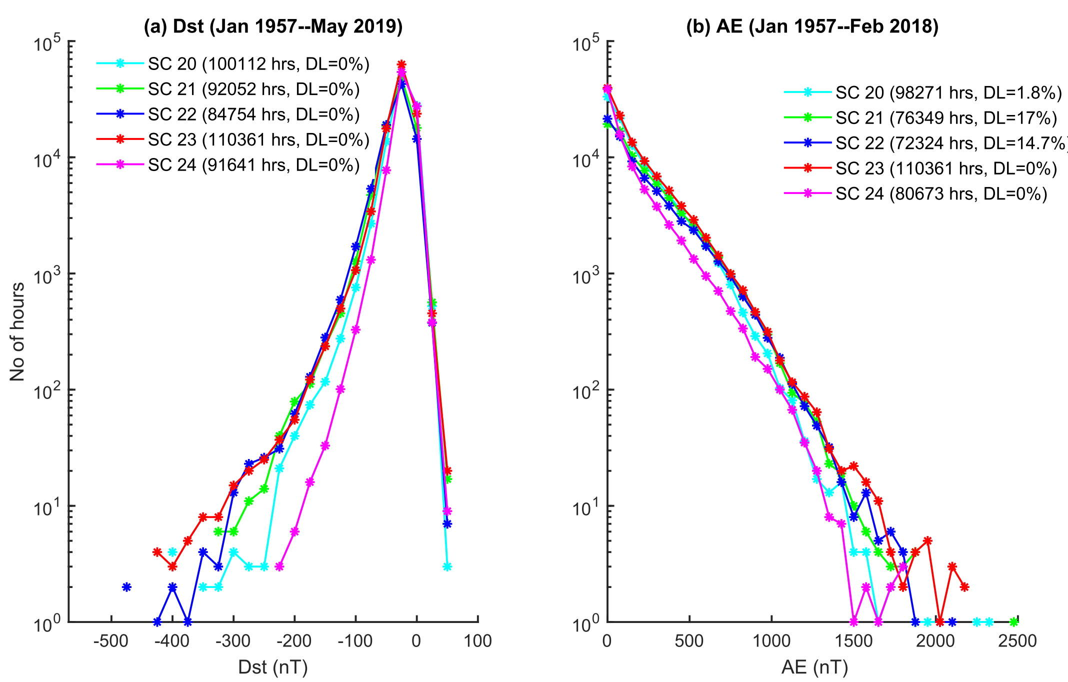

Fig. 2. (a) Probability distribution function associated with *Dst* index (a proxy for the strength of low-latitude ring current) for SCs 20–24. The number of intervals falling between different bins of *Dst* index are shown for SCs 20–24. (b) Probability distribution function associated with *AE* index (a proxy for the strength of high-latitude auroral electrojet current) for SCs 20–24. If we sum the individual PDF then we get total number of intervals for which data is available in that SC. The data loss for each SC is also mentioned in legend. If data loss is zero then summation of PDF will simply represent the length of SC in hours.

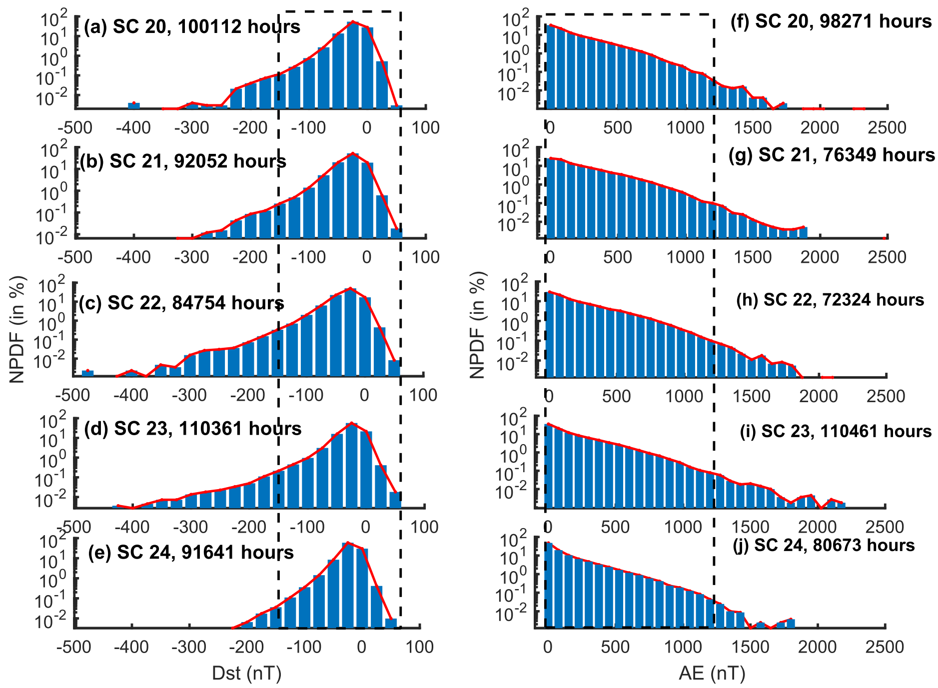

Fig. 3. (a)–(e) shows normalized probability distribution function (NPDF) associated with *Dst* index for SCs 20–24. (f)–(j) shows normalized probability distribution function (NPDF) associated with *AE* index for SCs 20–24. The probability of occurrence of one-hour intervals (in %) in different bins of *Dst* and *AE* are shown for SCs 20–24. If we sum the NPDF we get 100%, which corresponds to total number one-hour observations for each SC.

associated with ring-current and auroral electrojet current systems during SC 24. This implies presence of weaker ring-current and auroral electrojet current during SC 24 as compared to preceding SCs 20–23.

In general the periods with $Dst < -100$ nT considered to be associated with intense geomagnetic storm (Zhang et al., 2006). Thus, for further details we estimated the probability and total number of intervals with (i) $Dst < -150$ nT and (ii) $Dst < -250$ nT. The percentage occurrence of $Dst < -150$ nT and $Dst < -250$ nT for SCs 20–24 are plotted as a function of peak smoothed sunspot number in Fig. 4(a), and (b), respectively and their corresponding total number of one-hour intervals are depicted in Fig. 4 (c), and (d), respectively. It is found that number of total number of intervals with $Dst < -150$ nT are less than 600 h for SCs 20–23, and it covers maximum up to 0.7% of PDF. Whereas, intervals with $Dst < -250$ nT are found to be less than 100 h for SCs 20–23, which constitutes less than 0.1% of PDF. The interesting feature is observed during SC 24, the $Dst < -150$ nT encountered only for 58 h, which is only 0.06% of entire PDF. This percentage is one order less as compared to the percentages reported for SCs 20–23 for the limit of $Dst < -150$ nT. The probability of occurrence of $Dst < -150$ nT shows positive correlation with peak smoothed sunspot number (i.e.,S_m). Although correlation is based on five data points, the correlation is 0.92 and it is above 95% significance level. Whereas, the probability of occurrence of $Dst < -250$ nT does not show a clear dependence on peak smoothed sunspot number. It has a correlation of 0.66. Peak smoothed sunspot number is taken as the proxy for the strength of solar activity.

Similarly, we obtained the total intervals and their percentage for $AE > 750$ nT and $AE > 1500$ nT. The percentage occurrence of $AE > 750$ nT and $AE > 1500$ nT for SCs 20–24 are plotted as a function of peak smoothed sunspot number in Fig. 5(a), and (b), respectively and their corresponding total number of one-hour intervals are depicted in Fig. 5(c), and (d), respectively. It is found that the number of one-hour intervals with $AE > 750$ nT and $AE > 1500$ nT reached maximum up to 3060 and 70, respectively for SCs 20–23, which corresponds to maximum up to 4% and 0.06% of respective PDFs. But for SC 24 the $AE > 750$ nT encountered only for 1398 h i.e., 1.7% of PDF and there are only 9 intervals when AE increased above 1500 nT i.e., 0.01% of PDF. The probability of occurrence of $AE > 750$ nT shows positive correlation with peak smoothed sunspot number and gives the correlation coefficient of 0.96, which is above 95% significance level. Whereas, the probability of occurrence of $AE > 1500$ nT gives a correlation of 0.68. It suggest that the probability of occurrence of $AE > 1500$ nT does not show a clear dependence on peak smoothed sunspot number.

Variation in solar activity and subsequent modulation caused by the CMEs, CIRs, HSS etc to the interplanetary solar wind in the vicinity of the Earth's magnetosphere affects these current system. Thus, we examined the PDFs linked with interplanetary magnetic field Bz component, solar wind velocity and dawn-to-dusk component of the electric field at the Earth's bow shock nose for the SCs

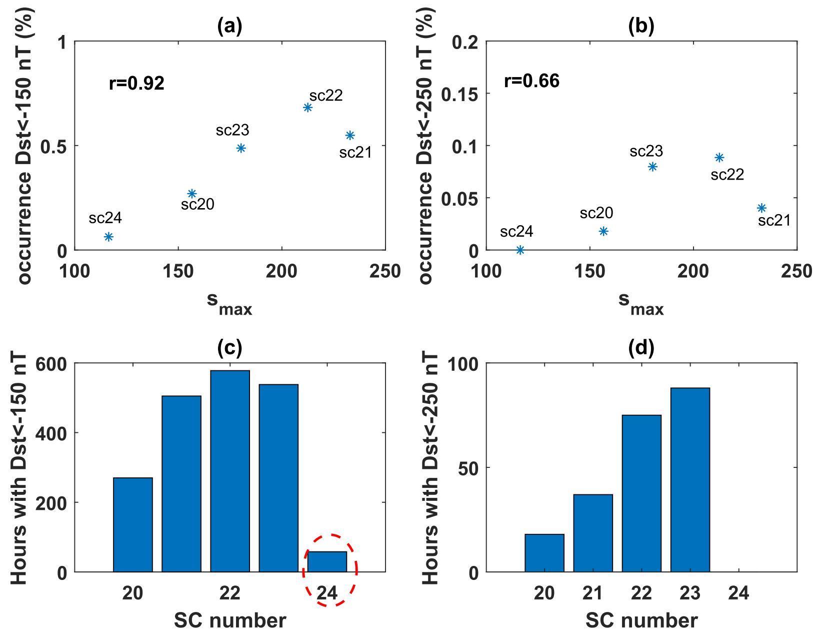

Fig. 4. The percentage occurrence of (a) $Dst < -150$ nT and (b) $Dst < -250$ nT for SCs 20–24 are plotted as a function of peak smoothed sunspot number (S_m) and their corresponding total number of one-hour intervals are depicted in panel (c) and (d), respectively.

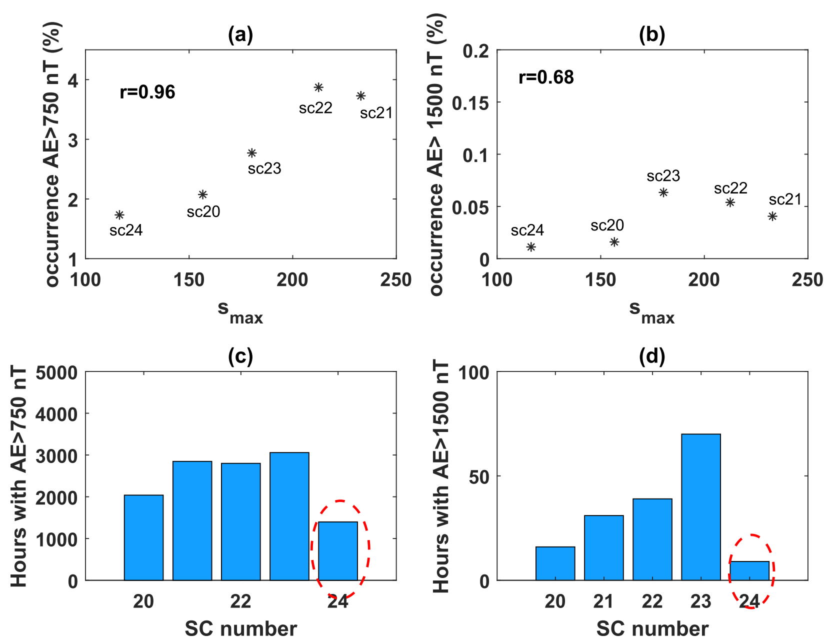

Fig. 5. The percentage occurrence of (a) $AE > 750$ nT and (b) $AE > 1500$ nT for SCs 20–24 are plotted as a function of peak smoothed sunspot number (S_m) and their corresponding total number of one-hour intervals are depicted in panel (c) and (d), respectively.

20–24. Particularly, for interplanetary parameters there is considerable data loss because of failure or saturation of space instruments during severe space weather conditions. For SCs 20–24 the NPDFs of IMF Bz (first column, a-e), solar wind velocity V (second column, f-j), and dawn-to-dusk electric field (third column, k-o) at Earth's bow shock nose are plotted in Fig. 6. The bin width for IMF Bz, V and Ey are taken as 4 nT, 50 km/s, and 4 mV/m, respectively. The number of one-hour intervals for which data was available are mentioned in respective plots with data loss (DL) percentage. For SCs 20–22 the data loss is more than 33%. For each parameter, for a given SC, if data loss exceeds 40% then it is shown by green color in Fig. 6. But for SCs 23 and 24 data loss is small (<0.2%). We have obtained number of intervals and their percentages in different limits for IMF Bz, solar wind velocity, and Ey, which are given in Table 1. For Bz we have taken two categories (i) $Bz < -12$ nT and (ii)$Bz < -20$ nT. For V we have considered (i) $V > 500$ km/s and (ii)$V > 700$ km/s and for Ey the categories are (i) $Ey > 8$ mV/m and (ii)$Ey > 16$ mV/

Please cite this article as: B. Kakad and A. Kakad, Characteristics of probability distribution functions of low- and high-latitude current systems during Solar Cycle 24, Advances in Space Research, https://doi.org/10.1016/j.asr.2019.12.021

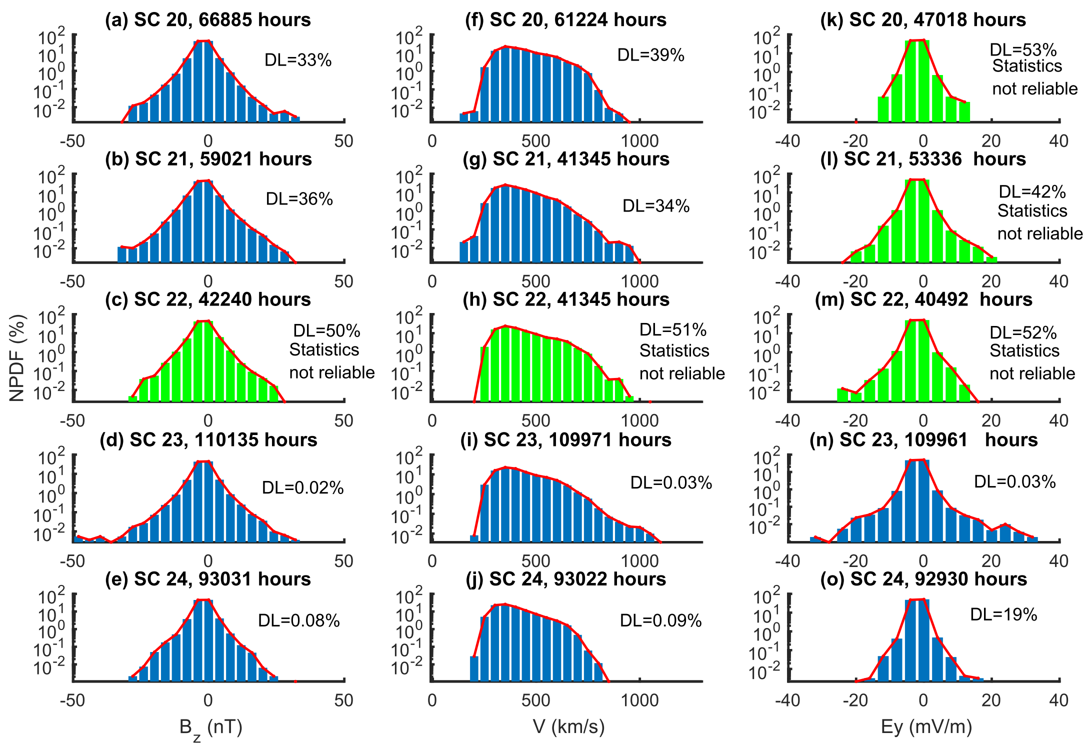

Fig. 6. For SCs 20–24 the NPDFs of IMF Bz (first column, a–e), solar wind velocity V (second column, f–j), and dawn-to-dusk electric field (third column, k–o) at Earth's bow shock nose are depicted. The number of one-hour intervals for which data was available are mentioned in respective plots with data loss percentages. The parameters for which data loss exceeds 40% is shown by green color. (For interpretation of the references to colour in this figure legend, the reader is referred to the web version of this article.)

m. The percentage occurrence and total duration in hours for these categories are summarized in Table 1. These estimates are not mentioned for the cases when data loss exceeds 40% because for such cases the computed statistics will not be reliable. This analysis clearly indicate significant reduction in time intervals with IMF $Bz < -12$ nT, solar wind velocity $V > 500$ km/s and $Ey > 8$ mV/m during SC 24 as compared to SC 23.

4. Discussion

Our study report that for SCs 20–23 the occurrence probability for $Dst < -150$ nT is found to be maximum up to 0.7% ($\approx<$ 600 h). It means over the entire period of the solar cycle, which is approximately 11 years, a period of less than 600 h encountered $Dst < -150$ nT. Whereas, for $AE > 750$ nT the occurrence probability is found to be maximum up to 4% ($\approx<$ 3060 h). The number of 0.7% for $Dst < -150$ (4% for $AE > 750$) looks negligible, but this is an extremely important component for the space weather studies. Because although the number of geomagnetically disturbed time intervals (i.e., $Dst < -150$ nT or $AE > 750$ nT) are less but it can cause severe impacts on our technology. So far the Carrington magnetic storm of 2 September 1859 with Dst reaching approximately -1600 nT is the intense space weather event known to us (Ngwira et al., 2014; Tsurutani et al., 2018). This super magnetic storm caused daytime aurora, which was visible even at low-latitudes (Hayakawa et al., 2016; Cid et al., 2015). Thus, even a few hours of the severe magnetic storm can cause significant damage to our space and ground-based technologies.

Table 1
It summarizes total one-hour intervals and their percentages for different categories, namely (i) IMF $Bz < -12$ nT and $Bz < -20$ nT, (ii) solar wind velocity, $V > 500$ km/s and $V > 700$ km/s, (iii) dawn-to-dusk interplanetary electric field $Ey > 8$ mV/m and $Ey > 16$ mV/m for SCs 20–24. These details are not mentioned for the parameters for which data loss is more than 40% in respective SCs. These interplanetary parameters represents the state of solar wind at Earth's bow shock nose.

SC No.	$Bz < -12$ nT % (No. of hrs)	$Bz < -20$ nT % (No. of hrs)	$V > 500$ km/s % (No. of hrs)	$V > 700$ km/s % (No. of hrs)	$Ey > 8$ mv/m % (No. of hrs)	$Ey > 16$ mV/m % (No. of hrs)
20	0.96% (640 h)	0.08% (54 h)	29.6% (18147 h)	2.9% (1765 h)	–	–
21	1.55% (920 h)	0.11% (63 h)	21.4% (13008 h)	1.1% (660 h)	–	–
22	–	–	–	–	–	–
23	1.21% (1330 h)	0.15% (155 h)	25.9% (28533 h)	2.2% (2410 h)	0.16% (174 h)	0.04% (42 h)
24	0.74% (694 h)	0.06% (56 h)	16.8% (15589 h)	0.54% (508 h)	0.05% (47 h)	0.00% (3 h)

Please cite this article as: B. Kakad and A. Kakad, Characteristics of probability distribution functions of low- and high-latitude current systems during Solar Cycle 24, Advances in Space Research, https://doi.org/10.1016/j.asr.2019.12.021

For the SC 24, the occurrence probability for $Dst < -150$ nT is only 0.06% (≈58 h). There is almost one order decrease in the durations associated with $Dst < -150$ nT. Whereas, the occurrence probability for $AE > 750$ nT is only 1.7% (≈1398 h). It implies that for the high latitude electrojet current system the intervals with $AE > 750$ have decreased nearly three times during SC 24 as compared to SCs 20–23. Overall, the present study implies the presence of fairly quiet space weather during SC 24. As mentioned earlier, the SCs 20–24 have experienced a gradual decrease in its activity and SC 24 is the weakest among them. Such a situation triggers the curiosity among scientists about the strength of upcoming SC 25. Recent studies suggest that SC 25 would be of the same amplitude as or slightly smaller than the SC 24 (Javaraiah, 2015; Cameron et al., 2016; Kakad et al., 2017; Singh and Bhargawa, 2017). If upcoming SC 25 happens to be weaker than SC 24 then we expect that the % occurrence of $Dst < -150$ nT ($AE > 750$ nT) will be considerably smaller than 58 h (1398 h) during SC 25. The quantitative estimates related to low-latitude ring current and high-latitude auroral electrojet systems presented here will be useful to understand the space weather scenario in the Earth's magnetosphere during past five SCs. This study was possible because of the availability of ring current and auroral electrojet information in the form of *Dst* and *AE* indices for more than five decades.

It is known that the behaviour and strength of IMF *Bz*, solar wind velocity and interplanetary dawn-to-dusk electric field play an important role in deciding the solar wind magnetosphere energy coupling through the process of magnetic reconnection. It is noted that PDFs of IMF *Bz*, solar wind velocity *V*, and dawn-to-dusk electric field are also considerably squeezed during SC 24. A significant reduction in time intervals with IMF $Bz < -12$ nT, $V > 500$ km/s and, $Ey > 8$ mV/m are observed during SC 24 as compared to SC 23. The IMF Bz, V and Ey did not cross the limit of −24 nT, 800 km/s, and 20 mV/m, respectively during SC 24. Recently, Watari (2017) examined daily occurrence rate of $Dst < -100$ nT during the ascending phase of SC 23 and 24 and found that the dawn-to-dusk electric field more frequently crosses a limit of 5 mV/m during SC 23 as compared to SC 24. Also, Zhuang et al. (2018) have reported that for CMEs faster than 1860 km/s the probability of CME caused geomagnetic storm with $Dst < -250$ nT is about 1/5 for SC 23 and 1/25 for SC 24. Thus, the likelihood of super intense geomagnetic storm ($Dst < -250$ nT) is significantly reduced during SC 24.

5. Summary and conclusions

In present study, behaviour of the probability distribution functions associated with the ring current and auroral electrojet current systems are examined for SCs 20–24 together with the PDFs linked with interplanetary solar wind parameters at the Earth's bow shock nose. Such a study was possible because of the availability of long-term *Dst* and *AE* observations for the past six SCs (i.e., from 19 to 24). Solar activity has experienced a gradual decrease in its strength since SC 20 and this decrease is the largest from SC 23 to SC 24 (Kakad et al., 2019; Ingale et al., 2019). Thus, we examined the probability distribution function associated with the ring-current and auroral electrojet current systems during this peculiar phase of the gradual decline of the solar activity. We have noticed significant narrowing in the probability distribution function of the ring-current and auroral electrojet current for SC 24 as compared to SCs 20–23. It suggests considerable decrease in the strength of ring-current and auroral electrojet current system during SC 24.

Overall there are approximately 600 h (100 h) that experienced $Dst < -150$ nT ($Dst < -250$ nT) during SCs 20–23. Whereas, for SC 24 there are only 58 h (0 h) when $Dst < -150$ nT ($Dst < -250$). Total period of 600 h (58 h) constitutes only 0.7% (0.06%) of the probability distribution function of SCs 20–23 (SC 24). We found that the probability of occurrence of $Dst < -150$ nT shows a positive correlation with the peak smoothed sunspot number (S_m) however, the probability of occurrence of $Dst < -250$ nT does not show a clear dependence on the smoothed sunspot number. The significant decrease in the intervals of $Dst < -150$ nT during SC 24 has its key in the solar wind-magnetosphere energy coupling. The solar wind-magnetosphere energy coupling is mainly controlled by the solar wind properties like its magnetic field, speed and the interplanetary electric field. Our analysis indicates that significant narrowing of the probability distribution function is also evident in IMF *Bz*, solar wind velocity and interplanetary dawn-to-dusk electric field during SC 24. Recently, it is reported that the energy transferred to the magnetosphere during the present SC 24 is only 46% of the energy transferred during SC 23 (Kakad et al., 2019). A study by Zhuang et al. (2018) also suggests that the likelihood of the occurrence of super geomagnetic storms ($Dst < -250$ nT) is significantly reduced in SC 24. The observed decrease in the intervals of $Dst < -150$ nT and $AE > 750$ nT during SC 24 is attributed to considerable step down in solar wind-magnetosphere energy coupling via reduced strength of IMF *Bz*, solar wind velocity and electric field during SC 24. If future SC happens to be weaker than SC 24 then we may not encounter geomagnetic storm with $Dst < -150$ nT and $AE > 750$ nT, in other words, the probability distribution function of the ring-current and auroral electrojet current systems may experience further narrowing.

Declaration of Competing Interest

The author declare that there is no conflict of interest.

Acknowledgement

We thank WDC Kyoto for geomagnetic activity index *Dst*, and SIDC SILSO for Version-II sunspot data and OMNIWEB for interplanetary solar wind data.

Please cite this article as: B. Kakad and A. Kakad, Characteristics of probability distribution functions of low- and high-latitude current systems during Solar Cycle 24, Advances in Space Research, https://doi.org/10.1016/j.asr.2019.12.021

References

Acero, F., Vaquero, J., Gallego, M., García, J., 2018. A limit for the values of the dst geomagnetic index. Geophys. Res. Lett. 45, 9435–9440.

Alves, M., Echer, E., Gonzalez, W., 2006. Geoeffectiveness of corotating interaction regions as measured by dst index. J. Geophys. Res.: Space Phys. 111.

Borovsky, J.E., Denton, M.H., 2006. Differences between cme-driven storms and cir-driven storms. J. Geophys. Res.: Space Phys. 111.

Burton, R.K., McPherron, R., Russell, C., 1975. An empirical relationship between interplanetary conditions and dst. J. Geophys. Res. 80, 4204–4214.

Cameron, R.H., Jiang, J., Schuessler, M., 2016. Solar cycle 25: another moderate cycle?. Astrophys. J. Lett. 823, L22.

Chapman, S., 1965. The ring current, geomagnetic storms and the auora. In: Proceedings of the Plasma Space Science Symposium. Springer, pp. 263–279.

Cid, C., Saiz, E., Guerrero, A., Palacios, J., Cerrato, Y., 2015. A carrington-like geomagnetic storm observed in the 21st century. J. Space Weather Space Clim. 5, A16.

Clette, F., Cliver, E., Lefèvre, L., Svalgaard, L., Vaquero, J., Leibacher, J., 2016. Preface to topical issue: recalibration of the sunspot number. Sol. Phys. 291, 2479–2486.

Cole, T., 1973. Periodicities in solar activity. Solar Phys. 30, 103–110.

Ebihara, Y., 2019. Simulation study of near-earth space disturbances: 2. Auroral substorms. Progr. Earth Planet. Sci. 6, 24.

Echer, E., Gonzalez, W., Guarnieri, F., Dal Lago, A., Vieira, L., 2005. Introduction to space weather. Adv. Space Res. 35, 855–865.

Echer, E., Rigozo, N., Nordemann, D., Vieira, L., 2004. Prediction of solar activity on the basis of spectral characteristics of sunspot number. Ann. Geophys. 22, 2239–2243.

Gonzalez, W., Echer, E., Clua-Gonzalez, A., Tsurutani, B., 2007. Interplanetary origin of intense geomagnetic storms (dst<- 100 nt) during solar cycle 23. Geophys. Res. Lett. 34.

Gonzalez, W., Joselyn, J.A., Kamide, Y., Kroehl, H.W., Rostoker, G., Tsurutani, B., Vasyliunas, V., 1994. What is a geomagnetic storm?. J. Geophys. Res.: Space Phys. 99, 5771–5792.

Gonzalez, W.D., Echer, E., Tsurutani, B.T., de Gonzalez, A.L.C., Dal Lago, A., 2011. Interplanetary origin of intense, superintense and extreme geomagnetic storms. Space Sci. Rev. 158, 69–89.

Hathaway, D., 2010. Living review in solar physics, 7, 1.

Hayakawa, H., Iwahashi, K., Tamazawa, H., Isobe, H., Kataoka, R., Ebihara, Y., Miyahara, H., Kawamura, A.D., Shibata, K., 2016. East asian observations of low-latitude aurora during the carrington magnetic storm. Publicat. Astronom. Soc. Japan 68.

Ingale, M., Janardhan, P., Bisoi, S., 2019. Beyond the mini-solar maximum of solar cycle 24: declining solar magnetic fields and the response of the terrestrial magnetosphere. J. Geophys. Res.: Space Phys.

Javaraiah, J., 2015. Long-term variations in the north–south asymmetry of solar activity and solar cycle prediction, iii: Prediction for the amplitude of solar cycle 25. New Astron. 34, 54–64.

Kakad, B., Kakad, A., Ramesh, D.S., 2017. Prediction of the length of upcoming solar cycles. Sol. Phys. 292, 181.

Kakad, B., Kakad, A., Ramesh, D.S., 2017. Shannon entropy-based prediction of solar cycle 25. Sol. Phys. 292, 95.

Kakad, B., Kakad, A., Ramesh, D.S., Lakhina, G.S., 2019. Diminishing activity of recent solar cycles (22–24) and their impact on geospace. J. Space Weather Space Clim. 9, A01.

Lakhina, G.S., Tsurutani, B.T., 2018. Supergeomagnetic storms: past, present, and future. Extreme Events in Geospace. Elsevier, 157–185.

Molinski, T.S., Feero, W.E., Damsky, B.L., 2000. Shielding grids from solar storms [power system protection]. IEEE Spectrum 37, 55–60.

Ngwira, C.M., Pulkkinen, A., Kuznetsova, M.M., Glocer, A., 2014. Modeling extreme carrington-type space weather events using three-dimensional global mhd simulations. J. Geophys. Res.: Space Phys. 119, 4456–4474.

Rawat, R., Echer, E., Gonzalez, W., 2018. How different are the solar wind-interplanetary conditions and the consequent geomagnetic activity during the ascending and early descending phases of the solar cycles 23 and 24?. J. Geophys. Res.: Space Phys. 123, 6621–6638.

Richardson, I., Webb, D., Zhang, J., Berdichevsky, D., Biesecker, D., Kasper, J., Kataoka, R., Steinberg, J., Thompson, B., Wu, C.C., et al., 2006. Major geomagnetic storms (dst <– 100 nt) generated by corotating interaction regions. J. Geophys. Res.: Space Phys. 111.

Richardson, I.G., 2013. Geomagnetic activity during the rising phase of solar cycle 24. J. Space Weather Space Clim. 3, A08.

Shen, C., Chi, Y., Wang, Y., Xu, M., Wang, S., 2017. Statistical comparison of the icme's geoeffectiveness of different types and different solar phases from 1995 to 2014. J. Geophys. Res.: Space Phys. 122, 5931–5948.

Singh, A., Bhargawa, A., 2017. An early prediction of 25th solar cycle using hurst exponent. Astrophys. Space Sci. 362, 199.

Tsurutani, B.T., Gonzalez, W., Lakhina, G., Alex, S., 2003. The extreme magnetic storm of 1–2 september 1859. J. Geophys. Res.: Space Phys. 108.

Tsurutani, B.T., Gonzalez, W.D., Kamide, Y., 1997. Magnetic storms. Surv. Geophys. 18, 363–383.

Tsurutani, B.T., Lakhina, G.S., Echer, E., Hajra, R., Nayak, C., Mannucci, A.J., Meng, X., 2018. Comment on modeling extreme carrington-type space weather events using three-dimensional global mhd simulations by cm ngwira, a. pulkkinen, mm kuznetsova, and a. glocer. J. Geophys. Res.: Space Phys. 123, 1388–1392.

Usoskin, I.G., 2017. A history of solar activity over millennia. Living Rev. Sol. Phys. 14, 3.

Watari, S., 2017. Geomagnetic storms of cycle 24 and their solar sources. Earth, Planets Space 69, 70.

Zhang, J., Liemohn, M.W., Kozyra, J.U., Thomsen, M.F., Elliott, H.A., Weygand, J.M., 2006. A statistical comparison of solar wind sources of moderate and intense geomagnetic storms at solar minimum and maximum. J. Geophys. Res.: Space Phys. 111.

Zhuang, B., Wang, Y., Shen, C., Liu, R., 2018. A statistical study of the likelihood of a super geomagnetic storm occurring in a mild solar cycle. Earth Planet. Phys. 2, 112–119.

Please cite this article as: B. Kakad and A. Kakad, Characteristics of probability distribution functions of low- and high-latitude current systems during Solar Cycle 24, Advances in Space Research, https://doi.org/10.1016/j.asr.2019.12.021